

Article

Study on Effect of High-Entropy Alloy Binder on Microstructure and Properties of WC Cemented Carbide Doped with Rare Earth Oxide

Yongqiang Qin ^{1,2,3}, Jian Yuan ¹, Yi Zhuang ¹, Bing Ma ¹, Laima Luo ^{1,2,3,*}  and Yucheng Wu ^{1,2,3,*}¹ School of Materials Science and Engineering, Hefei University of Technology, Hefei 230009, China² Engineering Research Center of High-Performance Copper Alloy Materials and Processing, Ministry of Education, Hefei 230009, China³ National-Local Joint Engineering Research Centre of Nonferrous Metals and Processing Technology, Hefei 230009, China

* Correspondence: luolaima@126.com (L.L.); ycwu@hfut.edu.cn (Y.W.)

Abstract: The AlCoCrFeNi powder was added to WC powder as a binder and Y₂O₃/ZrO₂ was doped by the wet chemical method as grain-growth inhibitors. The WC-Y₂O₃-ZrO₂-10AlCoCrFeNi composite powders were sintered by spark plasma sintering to obtain an alloy. The microstructure and properties of the cemented carbide were studied. The result showed that the rare-earth-oxide (Y₂O₃/ZrO₂)-refined grain size of the alloy and the high-entropy alloy binder provided the alloy with better hardness and toughness. The AlCoCrFeNi diffused slowly between the WC grains because of a delayed diffusion effect and Cr having a low affinity for the WC matrix. During the dynamic process of the WC particles' dissolution and precipitation growth, the Fe, Co, and Ni that had a better affinity for the WC matrix diffused and distributed more smoothly, which increased the strength and toughness of the alloy. When the temperature of the SPS sintering was 1250 °C, the WC-Y₂O₃-ZrO₂-10AlCoCrFeNi cemented carbide had the best properties, which was a Vickers hardness of 1888.14 HV and a fracture toughness of 14.76 MPa·m^{1/2}.

Keywords: WC-based cemented carbide; high-entropy alloy binder; rare earth oxide doping; spark plasma sintering



Citation: Qin, Y.; Yuan, J.; Zhuang, Y.; Ma, B.; Luo, L.; Wu, Y. Study on Effect of High-Entropy Alloy Binder on Microstructure and Properties of WC Cemented Carbide Doped with Rare Earth Oxide. *Coatings* **2023**, *13*, 273. <https://doi.org/10.3390/coatings13020273>

Academic Editor: Christian Mitterer

Received: 30 December 2022

Revised: 17 January 2023

Accepted: 18 January 2023

Published: 25 January 2023



Copyright: © 2023 by the authors. Licensee MDPI, Basel, Switzerland. This article is an open access article distributed under the terms and conditions of the Creative Commons Attribution (CC BY) license (<https://creativecommons.org/licenses/by/4.0/>).

1. Introduction

Cemented carbide materials are widely used in drilling tools, cutting tools, machining parts, and molds due to their excellent comprehensive mechanical properties. WC-based cemented carbide is among the most commonly used cemented carbide materials [1–3]. Cemented carbide materials made from a single WC have a high melting point and are difficult to sinter [4,5]. Therefore, cemented carbides used for high-performance cutting tools and wear-resistant parts are usually manufactured by adding a Co metal binder to induce liquid-phase sintering in WC. The combination of WC and Co provides WC-based cemented carbide with high hardness, sufficient fracture toughness, excellent wear resistance, and high temperature strength [6,7]. However, Co is a rare resource. In addition to the urgent need for Co in the field of cemented carbide, the demand for Co in many fields, such as the new lithium battery energy, is increasing; thus, the pressure on the supply of Co resources is increasing [8]. With the increasing use of cemented carbide materials, the property of traditional WC-Co cemented carbide has gradually failed to meet people's needs [9]. A high-entropy alloy can be added to cemented carbide WC and replace Co as a binder; the obtained hardness and fracture toughness are similar to those when Co is used as a binder [10]. To better obtain cemented carbide materials with excellent performance, a grain-growth inhibitor can be added to improve the mechanical properties of the alloy [11–16]. Therefore, the application of high-entropy alloys as a binder instead of

Co and a doping inhibitor has promising research significance in manufacturing WC-based cemented carbides.

High-entropy alloys (HEAs) usually consist of five or more elements and have high entropy, hysteresis diffusion, cocktail, and lattice distortion effects [17]. Through proper composition design, HEAs can potentially obtain better performance, such as improving the structure and magnetic properties of the material [18,19]. The cemented carbide prepared by using a high-entropy alloy instead of Co as the binder is a very feasible scheme to improve its material properties. AlCrFeCoNiV [14], (Al)CoCrCuFeNi [20,21], AlCoCrFeNi [22] and other high-entropy alloys have been applied in the field of cemented carbides. The high-entropy alloy AlCrFeCoNi was used as a binder of WC cemented carbide and inhibited the growth of WC grains, and the sintered alloy exhibited excellent hardness and fracture toughness [23].

The life of WC-based hard metal tools is extended by adding Y_2O_3 and ZrO_2 . Y_2O_3 can refine WC particles during carbonization and WC grains during sintering, thereby improving the hardness and fracture toughness [24]. ZrO_2 improves the uneven grain growth of WC-based cemented carbide, which gives the alloy a more uniform microstructure [25].

In this study, AlCoCrFeNi powders were used as the binder instead of Co and Y_2O_3/ZrO_2 was doped by the wet chemical method. WC- Y_2O_3 - ZrO_2 -10AlCoCrFeNi composite powders were mixed by ball milling and sintered by spark plasma sintering. The effect of the HEA binder on the microstructure and properties of the WC- Y_2O_3 - ZrO_2 -10AlCoCrFeNi material was studied. Additionally, optimum sintering parameters were also discussed to provide the alloy with better performance.

2. Experimental Method

2.1. Materials Preparation

The WC- Y_2O_3 - ZrO_2 -10AlCoCrFeNi composite powder was composed of 90% WC- Y_2O_3 - ZrO_2 (WC 99.6%, Y_2O_3 0.25%, ZrO_2 0.15%) and 10% AlCoCrFeNi. The morphologies of the starting powder are shown in Figure 1.

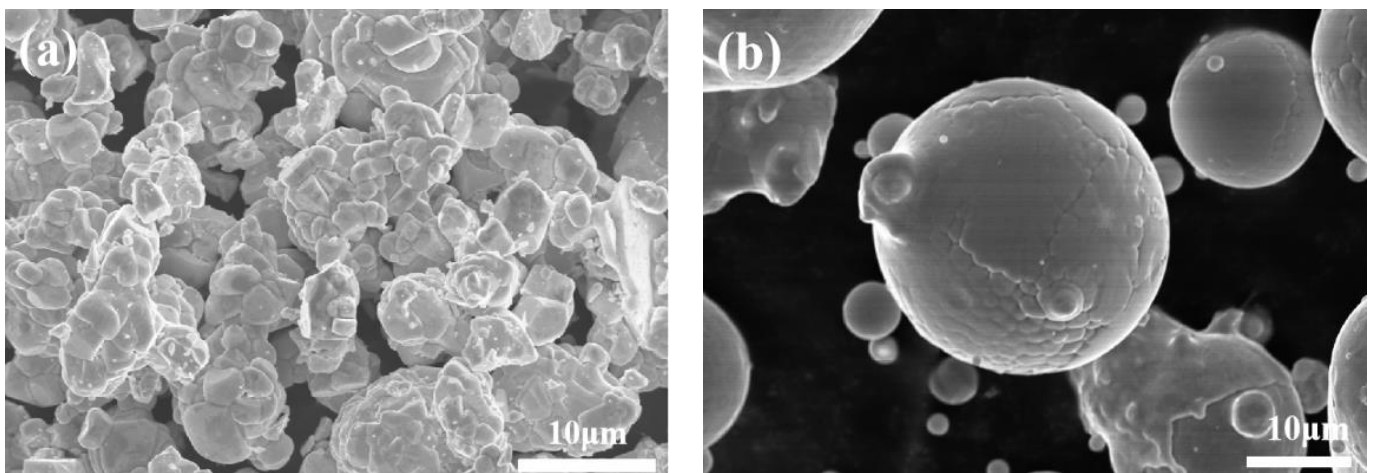


Figure 1. SEM (SE) images of raw materials. (a) WC- Y_2O_3 - ZrO_2 powder; (b) AlCoCrFeNi powder.

The WC- Y_2O_3 - ZrO_2 -10AlCoCrFeNi cemented carbide powder was prepared by the following steps [26,27]. (a) Dry ball milling: WC- Y_2O_3 - ZrO_2 powder, AlCoCrFeNi powder, and balls were poured into the ball mill tank for encapsulation in the glove box filled with argon gas. The ball powder mass ratio of 8:1 was used in the QM-QX4 type omnidirectional planetary ball mill. The milling speed was 150 r/min, and the milling time was 1800 min. (b) Wet ball milling: With ethanol as the liquid medium, the ball milling of WC- Y_2O_3 - ZrO_2 -10AlCoCrFeNi powder was mixed for 120 min. (c) Drying: The wet, ground solid-liquid mixture was poured into a beaker and placed in a DHG-9070 electric heating air-blowing drying oven at a constant temperature of 140 °C for 720 min. (d) Spark plasma sintering:

The cemented carbide powder was pressed into a graphite mold with a diameter of 20 mm and then placed in the vacuum chamber of the SPS furnace. The pre-pressure was set at 20 MPa and was slowly increased to 50 MPa during sintering. Sintering temperatures were 1200–1300 °C and the holding time was 5 min. The heating and cooling rate of the whole sintering process was 100 °C/min. The temperature was increased to 600 °C to discharge the residual air in the powder and was maintained at this level for 5 min. The above experimental process is shown in Figure 2.

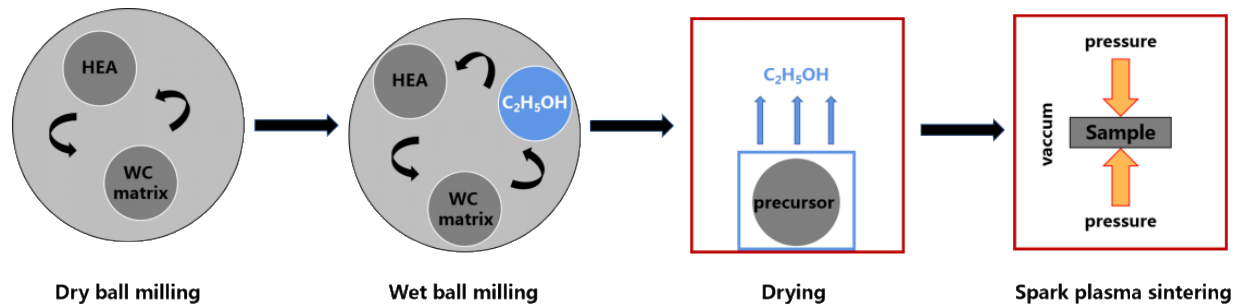


Figure 2. Schematic diagram of preparation process of the WC-Y₂O₃-ZrO₂-AlCoCrFeNi cemented carbide.

2.2. Sample Characterization

Fixed-target X-ray diffraction (XRD; Cu-K α ; PANalytical X-Pert PRO MPD, Holland) was used to study the WC-Y₂O₃-ZrO₂-10AlCoCrFeNi and WC-10AlCoCrFeNi powders and their alloys. Scanning electron microscopy (FE-SEM; SU8020, Japan) was used to analyze the microstructures of the mixed powder. Transmission electron microscopy (FE-TEM; FEI Tecnai G2 F20 S-TWIN, USA) was used for the analysis of the WC-Y₂O₃-ZrO₂-10AlCoCrFeNi alloy. Image analysis software Nano Measurer 1.2 was used to obtain the WC grain size distribution and average grain size of the sintered alloy. More than 400 WC grains per sample were used for statistics. The density of the cemented carbide was measured by the Archimedes drainage method. The hardness of the alloy was measured using a Vickers hardness tester, with holding time of 15 s and a load of 10 kg. The fracture toughness (K_{IC}) was calculated from the crack lengths measured by the Vickers indentation by [24]:

$$K_{IC} = 0.028 \sqrt{\frac{HvP}{\Sigma L}} \quad (1)$$

where K_{IC} is the fracture toughness, Hv is Vickers hardness, P is 10 kg, and L is the length of cracks at the four corners of the indentation. The surface of the samples was polished to mirror finish prior to indenting.

3. Results and Discussion

3.1. Microstructure and Composition of WC-Y₂O₃-ZrO₂-10AlCoCrFeNi Powder

Figure 3 shows the XRD pattern of the WC-Y₂O₃-ZrO₂-10AlCoCrFeNi composite powder, showing that the diffraction peaks in the figure were mainly in the WC phase. This was because the content of WC was much higher than that of the other phases to form this diffraction peak phenomenon.

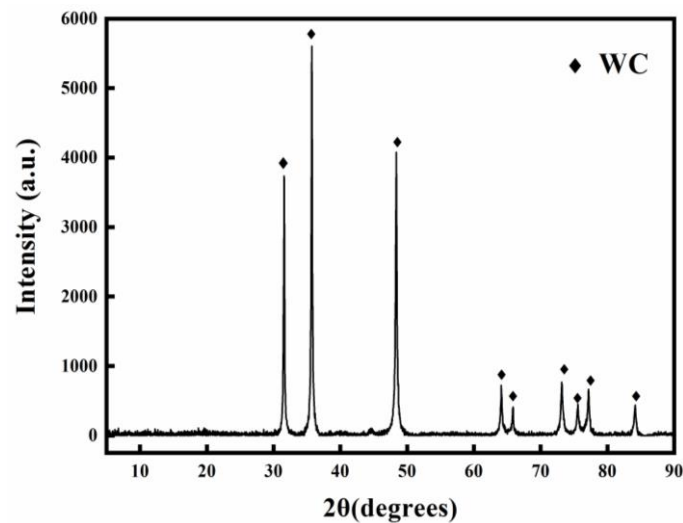


Figure 3. XRD pattern of the WC-Y₂O₃-ZrO₂-10AlCoCrFeNi composite powder.

Figure 4 shows the morphology of the WC-Y₂O₃-ZrO₂-10AlCoCrFeNi composite polyhedral powder. The shape of the WC-Y₂O₃-ZrO₂-10AlCoCrFeNi composite powder was irregular and some small particles were attached to the surface of the larger particles. In the ball milling process, the particle size of the WC-Y₂O₃-ZrO₂ powder differed greatly from that of the AlCoCrFeNi powder, and the texture of the WC-Y₂O₃-ZrO₂ powder particles were hard and brittle, so the powder particles were broken due to collision [28].

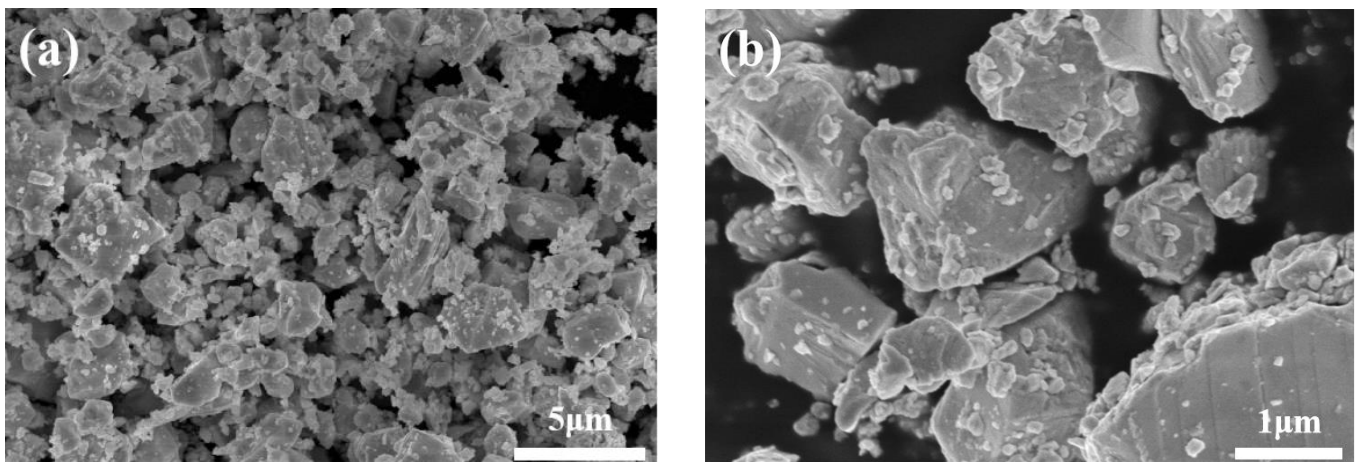


Figure 4. SEM (SE) images of WC-Y₂O₃-ZrO₂-10AlCoCrFeNi powder. (a) 5000 ×; (b) 20,000 ×.

3.2. Effect of Sintering Temperature on WC-Y₂O₃-ZrO₂-10AlCoCrFeNi Cemented Carbides

Figure 5 shows the XRD patterns of the WC-Y₂O₃-ZrO₂-10AlCoCrFeNi cemented carbide at 1200 °C, 1250 °C, and 1300 °C, showing only clear peaks for the WC phase.

Figure 6 shows the morphology and WC particle size distribution of the WC-Y₂O₃-ZrO₂-10AlCoCrFeNi cemented carbide at different sintering temperatures. Figure 6a,d show that at a sintering temperature of 1200 °C, the average WC grain size was 0.88 μm. Figure 6b,e show that sintering at 1250 °C caused no discernable porosity. The average size of the WC crystal grains was 0.70 μm. Figure 6c,f, at a sintering temperature of 1300 °C, show some abnormally coarse WC grains. The average size of the WC crystal grains was 1.01 μm.

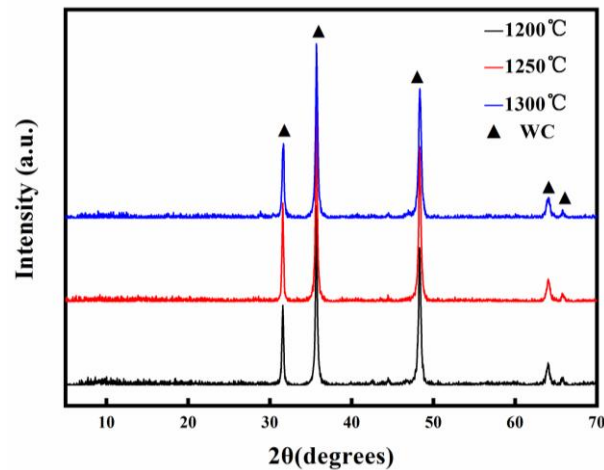


Figure 5. XRD patterns from the WC-Y₂O₃-ZrO₂-10AlCoCrFeNi cemented carbide sintered at different temperatures.

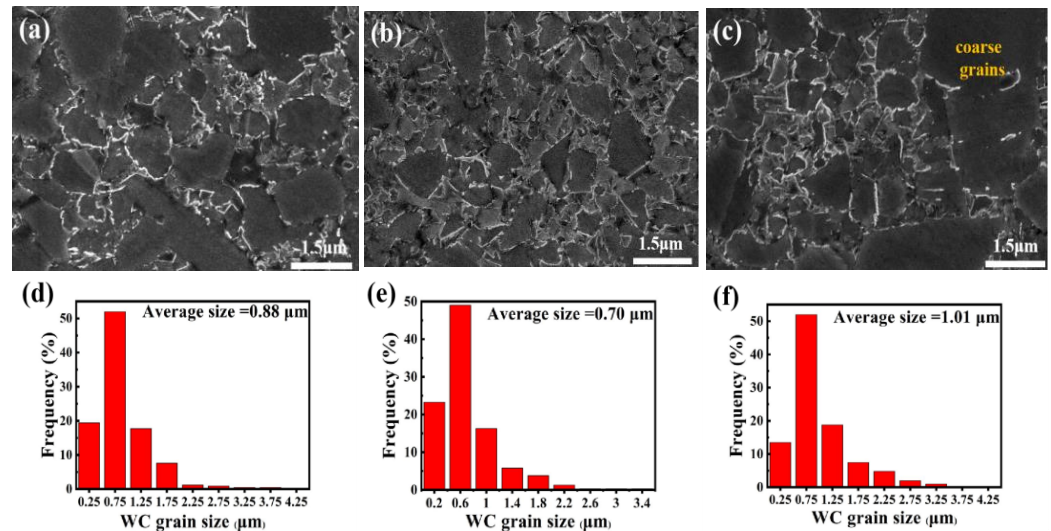


Figure 6. SEM (SE) images and size distributions of WC grains of the WC-Y₂O₃-ZrO₂-10AlCoCrFeNi cemented carbide prepared at: (a,d) 1200 °C, (b,e) 1250 °C, and (c,f) 1300 °C.

Thus, at 1250 °C, the WC-Y₂O₃-ZrO₂-10AlCoCrFeNi had almost no holes. The most uniform WC grain distribution and the smallest grain size occurred at 1250 °C. Sintering at 1200 °C did not allow some small grains to fully combine to form large grains, so the WC grains showed an uneven distribution [20,29,30]. When the sintering temperature was increased to 1300 °C, grain coarsening occurred. When the sintering temperature reached 1250 °C, the alloy was fully sintered, with almost no porosity. Therefore, at this sintering temperature, the alloy had the lowest porosity, the most uniform WC grain distribution, and the smallest grain size.

Figure 7 shows the densities of the WC-Y₂O₃-ZrO₂-10AlCoCrFeNi cemented carbide at different sintering temperatures. At 1250 °C, the highest actual and relative densities were obtained. This showed that the binder phase had good wettability. Thus, it was fully sintered, with good densification effect.

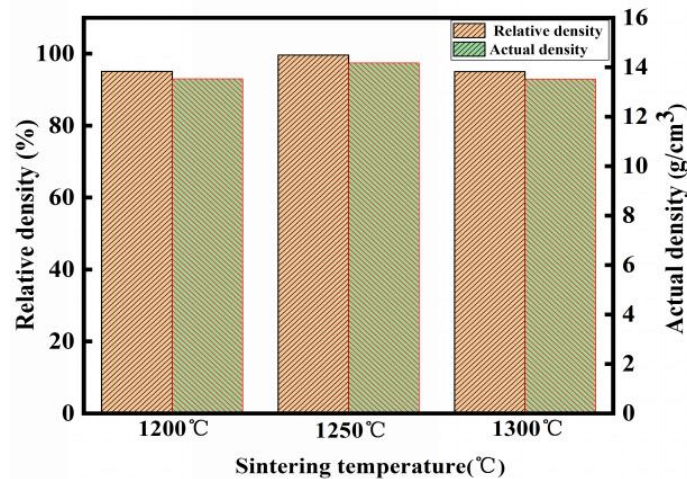


Figure 7. Density of the WC-Y₂O₃-ZrO₂-10AlCoCrFeNi cemented carbide at different sintering temperatures.

Figure 8 shows the hardness and fracture toughness of the WC-Y₂O₃-ZrO₂-10AlCoCrFeNi cemented carbide at different sintering temperatures. The best hardness and fracture toughness were obtained at a sintering temperature of 1250 °C.

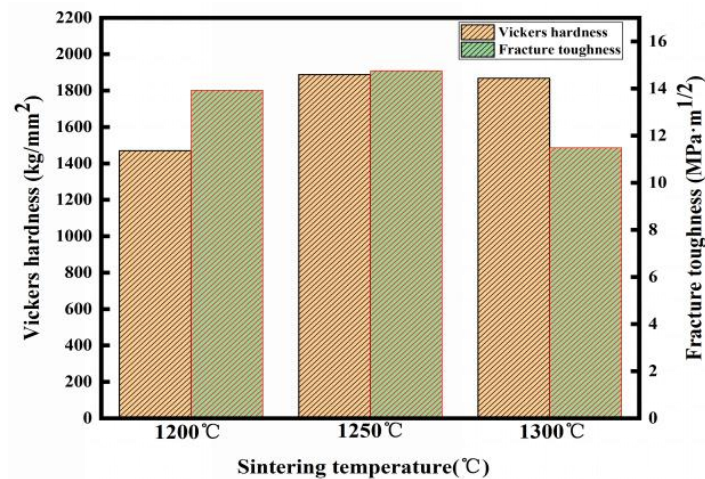


Figure 8. Vickers hardness and fracture toughness of the WC-Y₂O₃-ZrO₂-10AlCoCrFeNi cemented carbide at different sintering temperatures.

The best properties of the WC-Y₂O₃-ZrO₂-10AlCoCrFeNi cemented carbide were obtained at a sintering temperature of 1250 °C by using SPS.

3.3. Microstructure of WC-Y₂O₃-ZrO₂-10AlCoCrFeNi

Figure 9 shows the HAADF-STEM image and EDX maps of the WC-Y₂O₃-ZrO₂-10AlCoCrFeNi cemented carbide. Figure 9a–c show that the main component of the dark area in Figure 9a was the binder AlCoCrFeNi, and the main component of the bright area was the WC. The EDX analysis of the dark area #1 and the bright area #2 showed that the high-entropy binder AlCoCrFeNi was uniformly dispersed between the WC grains, and Al, Co, Cr, Fe, Ni, and other elements were almost undetectable in the WC grains, showing that AlCoCrFeNi had hardly diffused in the WC grains. AlCoCrFeNi diffuses slowly within the WC matrix due to the delayed diffusion effect of the high-entropy alloy AlCoCrFeNi, thereby inhibiting the growth of WC grains and improving the hardness and fracture toughness of the alloy [21,31,32].

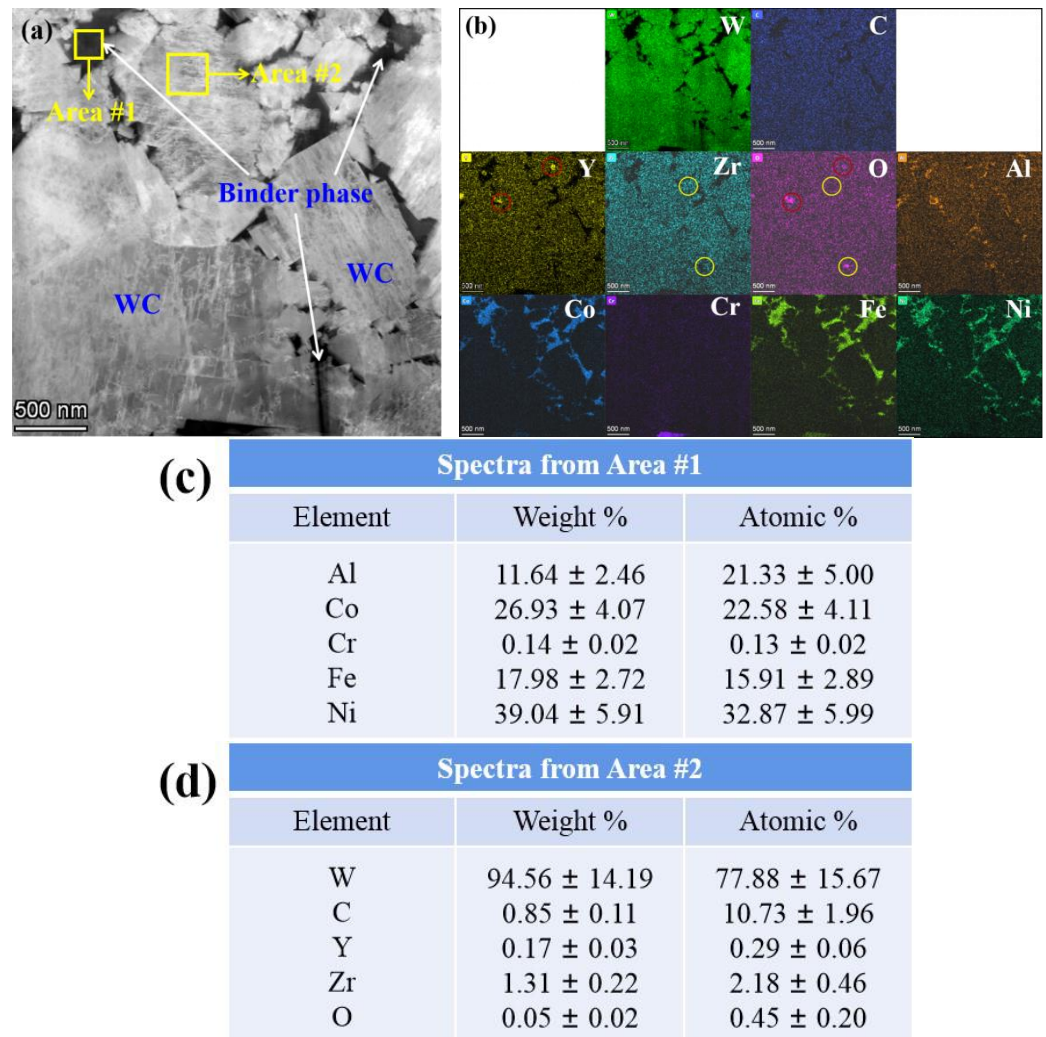


Figure 9. HAADF-STEM image and EDX mapping of the WC-Y₂O₃-ZrO₂-10AlCoCrFeNi cemented carbide: (a) HAADF-STEM image; (b) the corresponding elemental mappings of W, C, Y, Zr, O, Al, Co, Cr, Fe and Ni; (c) EDX from Area #1; (d) EDX from Area #2.

The enrichment of Y, Zr, and O elements was observed in the distribution of elements, indicating that Y and Zr existed in the form of oxides in the alloy [33–35]. In the rare-earth-oxide-modified WC-based cemented carbides, the rare earth oxide was dispersed in the grain boundary in the form of the second phase, which had a pinning effect and a dispersion-strengthening effect on the alloy grains, thereby improving the overall integration of the alloy's mechanical properties.

Figure 10 shows high-resolution TEM and line scans of the WC-Y₂O₃-ZrO₂-10AlCoCrFeNi cemented carbide. Figure 10a shows the high intensity of W in the grains and the low intensity of high-entropy alloying elements. The intensity of the W element in the binder phase was low, and the intensity of the high-entropy alloying elements was more obvious. The intensity of Al, Fe, Co, and Ni was evenly distributed at the WC grain boundaries, and the intensity of chromium was in the middle area. This indicated that chromium had a low affinity for the WC.

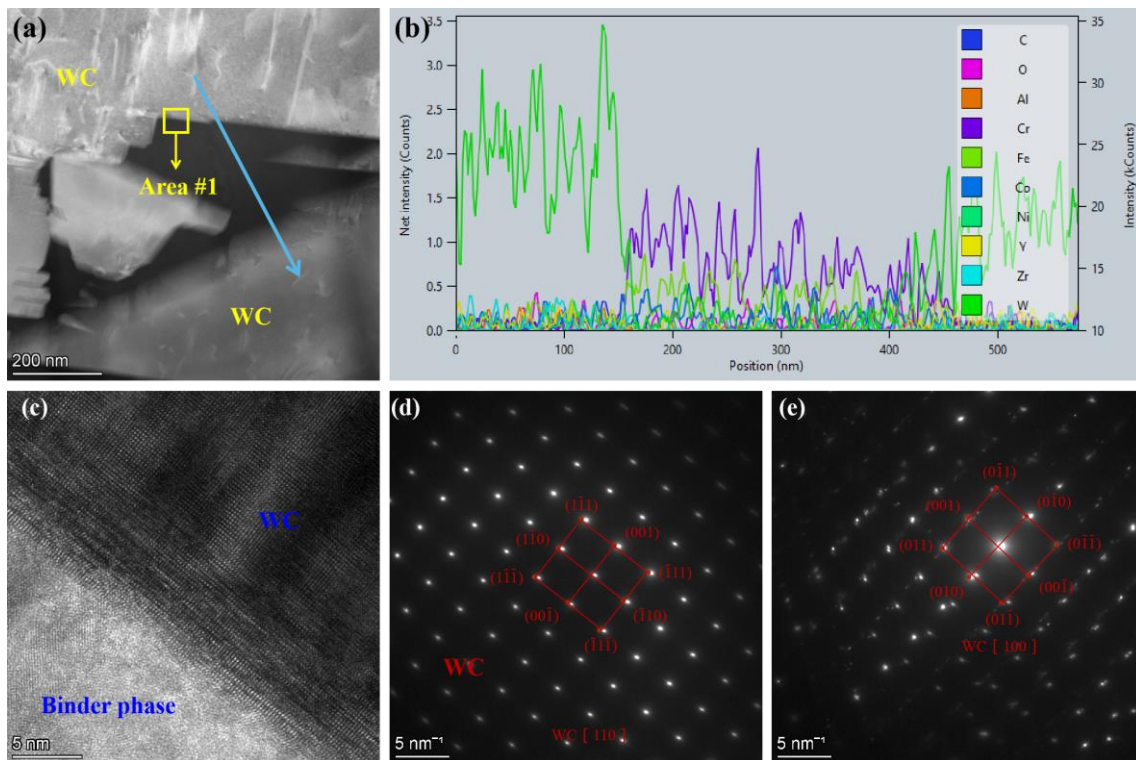


Figure 10. TEM images of the WC- Y_2O_3 - ZrO_2 -10AlCoCrFeNi cemented carbide: (a) HAADF-STEM image, (b) line scan, (c) high-resolution image, (d) diffraction pattern on WC grain, and (e) binder phase near WC grain partially diffracted spots.

In the dynamic process of WC particle dissolution and precipitation growth, the Fe, Co, and Ni that diffused to the WC grain surface had a better affinity for the WC, which increased the strength and toughness of the alloy [36–40].

Diffraction spot analysis was performed on a WC grain and binder phase near the WC grain, and the results are shown in Figure 10d,e. The diffraction pattern in Figure 10d indicates that the WC grains had a hexagonal crystal structure, whereas Figure 10e shows scattered diffraction spots different from WC phases in addition to hexagonal crystalline WC phases. This finding shows that the AlCoCrFeNi and WC- Y_2O_3 - ZrO_2 matrixes had good wettability and bonding, thereby improving the fracture toughness of the WC- Y_2O_3 - ZrO_2 -10AlCoCrFeNi cemented carbide.

Figure 11 shows the comparison properties for WC- Y_2O_3 - ZrO_2 -10AlCoCrFeNi, WC-10AlCoCrFeNi, and WC- Y_2O_3 - ZrO_2 -10Co cemented carbides. The actual density of WC- Y_2O_3 - ZrO_2 -10AlCoCrFeNi cemented carbide was 14.18 g/cm^3 , the density was 99.65%, the Vickers hardness was 1888.14 HV, and the fracture toughness was $14.76 \text{ MPa}\cdot\text{m}^{1/2}$. Compared with the WC-10AlCoCrFeNi cemented carbide, the density was slightly increased, the Vickers hardness was increased by 12.97%, and the fracture toughness was increased by 30.62%. Compared with the WC- Y_2O_3 - ZrO_2 -10Co cemented carbide, the density was almost unchanged, the Vickers hardness increased by 50.28%, and the fracture toughness increased by 18.46%.

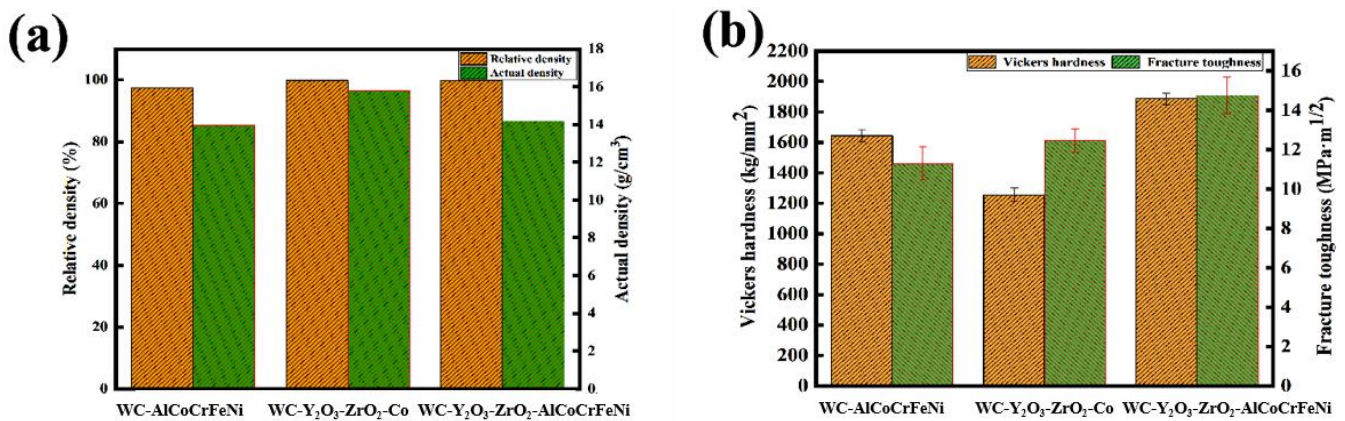


Figure 11. Comparison of properties of the WC-Y₂O₃-ZrO₂-10AlCoCrFeNi cemented carbide with WC-10AlCoCrFeNi and WC-Y₂O₃-ZrO₂-10Co cemented carbides: (a) relative and actual densities and (b) Vickers hardness and fracture toughness.

4. Conclusions

A WC-Y₂O₃-ZrO₂-10AlCoCrFeNi cemented carbide with excellent properties was obtained by ball milling and discharge plasma sintering. The influence of sintering temperature on the microstructure and properties of the WC-Y₂O₃-ZrO₂-10AlCoCrFeNi cemented carbide was studied, and the following conclusions were drawn:

- (1) A highly densified WC-Y₂O₃-ZrO₂-10AlCoCrFeNi cemented carbide was obtained by spark plasma sintering technology. Among the three samples of WC-Y₂O₃-ZrO₂-10AlCoCrFeNi cemented carbide sintered at 1200 °C, 1250 °C, and 1300 °C, the WC grains of the alloy were smallest, the densification achieved the best effect, and the hardness and fracture toughness were the best in the sample sintered at 1250 °C.
- (2) AlCoCrFeNi diffused slowly within the WC matrix due to the delayed diffusion effect of the high-entropy alloy AlCoCrFeNi, which inhibited the growth of the WC grains and improved the hardness and fracture toughness of the alloy. Chromium had a low affinity for the WC. During the dynamic process of the WC particle dissolution and precipitation growth, the Fe, Co, and Ni that diffused to the WC grain surface had a better affinity for the WC, which increased the strength and toughness of the alloy. The WC-Y₂O₃-ZrO₂-10AlCoCrFeNi cemented carbide had an extremely high density, with a Vickers hardness of 1888.14 HV and fracture toughness of 14.76 MPa·m^{1/2}. Compared with WC-10AlCoCrFeNi and WC-Y₂O₃-ZrO₂-10Co, the Vickers hardness increased by 12.97% and 50.28%, and the fracture toughness increased by 30.62% and 18.46%, respectively.

Author Contributions: Concept, Y.Q. and J.Y.; Method, J.Y.; Investigation, Y.Q., J.Y. and Y.Z.; Analysis, J.Y., B.M. and Y.Q.; Writing of draft, J.Y.; Writing editing, Y.Q. and J.Y.; Supervision, L.L. and Y.W.; Project management, Y.Q., L.L. and Y.W. All authors have read and agreed to the published version of the manuscript.

Funding: This research was funded by the Natural Science Foundation of Anhui Province grant number 2208085ME122, 2108085J21, National Key Research and Development Program of China grant number 2019YFE03120002, National Key Research and Development Program of Anhui Province grant number 202103a05020002, The Opening Foundation of National Joint Engineering Research Center for Abrasion Control and Molding of Metal Materials grant number HKDNM2021018 and the Higher Education Discipline Innovation Project “New Materials and Technology for Clean Energy” grant number B18018.

Acknowledgments: The authors gratefully acknowledge the support by Hefei University of Technology, Engineering Research Center of High-Performance Copper Alloy Materials and Processing of Ministry of Education and National-Local Joint Engineering Research Centre of Nonferrous Metals and Processing Technology.

Conflicts of Interest: The authors declare no conflict of interest.

References

1. Roa, J.J.; Phani, P.S.; Oliver, W.C.; Llanes, L. Mapping of mechanical properties at microstructural length scale in WC-Co cemented carbides: Assessment of hardness and elastic modulus by means of high speed massive nanoindentation and statistical analysis. *Int. J. Refract. Met. Hard Mater.* **2018**, *75*, 211–217. [[CrossRef](#)]
2. Wang, S.; Li, Y.M.; Wang, J.; Zheng, Z.B.; Luo, T.G.; Zheng, K.H.; Long, J. Effect of sintering temperature on the microstructure and properties of Ti/W-C reinforced Fe-based composites. *Vacuum* **2021**, *194*, 110617. [[CrossRef](#)]
3. Xu, B.P.; Zhou, Y.C.; Liu, Y.D.; Hu, S.J.; Zhang, G.D. Effect of different contents of WC on microstructure and properties of CrMnFeCoNi high-entropy alloy-deposited layers prepared by PTA. *J. Mater. Res.* **2022**, *37*, 719–727. [[CrossRef](#)]
4. Chen, Z.W.; Wang, Z.H.; Wang, B.X.; Yuan, J.T.; Huang, L.; Yin, Z.B. Microstructure and properties of WC-8Co cemented carbides prepared by multiple spark plasma sintering. *Int. J. Appl. Ceram. Technol.* **2021**, *18*, 2010–2019. [[CrossRef](#)]
5. Sun, J.L.; Huang, Z.F.; Zhao, J. High-hard and high-tough WC-TiC-Co cemented carbide reinforced with graphene. *Mater. Today Commun.* **2021**, *29*, 102841. [[CrossRef](#)]
6. Liu, K.; Wang, Z.H.; Yin, Z.B.; Cao, L.Y.; Yuan, J.T. Effect of Co content on microstructure and mechanical properties of ultrafine grained WC-Co cemented carbide sintered by spark plasma sintering. *Ceram. Int.* **2018**, *44*, 18711–18718. [[CrossRef](#)]
7. Lv, Z.P.; Wu, Y.J.; Dang, J.; Liu, D.; Hu, L.W.; Du, K.P.; Sun, H.B. Effect of yttrium on morphologies and size of tungsten carbide particles prepared through CO reduction. *J. Mater. Res. Technol.* **2020**, *9*, 10166–10174. [[CrossRef](#)]
8. Yu, B.H.; Li, Y.P.; Lei, Q.; Nie, Y. Microstructures and mechanical properties of WC-Co-xCr-Mo cement carbides. *J. Alloy. Compd.* **2019**, *771*, 636–642. [[CrossRef](#)]
9. Kresse, T.; Meinhard, D.; Bernthaler, T.; Schneider, G. Hardness of WC-Co hard metals: Preparation, quantitative microstructure analysis, structure-property relationship and modelling. *Int. J. Refract. Met. Hard Mater.* **2018**, *75*, 287–293. [[CrossRef](#)]
10. Ocak, B.C.; Goller, G. Investigation the effect of FeNiCoCrMo HEA addition on properties of B₄C ceramic prepared by spark plasma sintering. *J. Eur. Ceram. Soc.* **2021**, *41*, 6290–6301. [[CrossRef](#)]
11. Li, J.M.; Li, X.Q.; Xia, X.J. Effects of Al₂O₃-ZrO₂ content on the densification, microstructure, and mechanical properties of cemented tungsten carbides. *Mater. Chem. Phys.* **2022**, *276*, 125330. [[CrossRef](#)]
12. He, S.W.; Wang, M.H.; Bai, Q.; Xia, S.; Zhou, B.X. Effect of TaC Content on Microstructure and Mechanical Properties of WC-TiC-TaC-Co Cemented Carbide. *Acta Metall. Sin.* **2020**, *56*, 1015–1024.
13. Khuengpukheiw, R.; Wisitsoraat, A.; Saikaew, C. Wear behaviors of HVOF-sprayed NiSiCrFeB, WC-Co/NiSiCrFeB and WC-Co coatings evaluated using a pin-on-disc tester with C45 steel pins. *Wear* **2021**, *484*, 203699. [[CrossRef](#)]
14. Solodkyi, I.; Teslia, S.; Bezdorozhev, O.; Trosnikova, I.; Yurkova, O.; Bogomol, I.; Loboda, P. Hardmetals prepared from WC-W₂C eutectic particles and AlCrFeCoNiV high entropy alloy as a binder. *Vacuum* **2022**, *195*, 110630. [[CrossRef](#)]
15. Edtmaier, C.; Wolf, M.; Calderon, R.D.; Schubert, W.D. Effect of nickel on the formation of gamma/gamma' microstructures in WC/Co-Ni-Al-W. *Int. J. Refract. Met. Hard Mater.* **2021**, *100*, 105652. [[CrossRef](#)]
16. Zhang, H.; Xiong, J.; Guo, Z.X.; Yang, T.N.; Liu, J.B.; Hua, T. Microstructure, mechanical properties, and cutting performances of WC-Co cemented carbides with Ru additions. *Ceram. Int.* **2021**, *47*, 26050–26062. [[CrossRef](#)]
17. Yadav, S.; Zhang, Q.F.; Behera, A.; Haridas, R.S.; Agrawal, P.; Gong, J.D.; Mishra, R.S. Role of binder phase on the microstructure and mechanical properties of a mechanically alloyed and spark plasma sintered WC-FCC HEA composites. *J. Alloy Compd.* **2021**, *877*, 160265. [[CrossRef](#)]
18. Vinnik, D.A.; Zhivulin, V.E.; Trofimov, E.A.; Gudkova, S.A.; Punda, A.Y.; Valiulina, A.N.; Gavriyak, M.; Zaitseva, O.V.; Taskaev, S.V.; Khandaker, M.U.; et al. A-site cation size effect on structure and magnetic properties of Sm(Eu,Gd)Cr_{0.2}Mn_{0.2}Fe_{0.2}Co_{0.2}Ni_{0.2}O₃ high entropy solid solutions. *Nanomaterials* **2022**, *12*, 36. [[CrossRef](#)]
19. Zhivulin, V.E.; Sherstyuk, D.P.; Zaitseva, O.V.; Cherkasova, N.A.; Vinnik, D.A.; Taskaev, S.V.; Trofimov, E.A.; Trukhanov, S.V.; Latushka, S.I.; Tishkevich, D.I.; et al. Creation and magnetic study of ferrites with magnetoplumbite structure multisubstituted by Al³⁺, Cr³⁺, Ga³⁺, and In³⁺ cations. *Nanomaterials* **2022**, *12*, 1306. [[CrossRef](#)]
20. Mueller-Grunz, A.; Alveen, P.; Rassbach, S.; Useldinger, R.; Moseley, S. The manufacture and characterization of WC-(Al)CoCrCuFeNi cemented carbides with nominally high entropy alloy binders. *Int. J. Refract. Met. Hard Mater.* **2019**, *84*, 105032. [[CrossRef](#)]
21. Luo, W.Y.; Liu, Y.Z.; Luo, Y.; Wu, M. Fabrication and characterization of WC-AlCoCrCuFeNi high-entropy alloy composites by spark plasma sintering. *J. Alloy Compd.* **2018**, *754*, 163–170. [[CrossRef](#)]
22. Wei, Z.; Wu, Y.P.; Hong, S.; Cheng, J.B.; Qiao, L.; Ceng, J.; Zhu, S.S. Electrochemical properties and cavitation erosion behaviors of HVOF sprayed (AlCoCrFeNi)(1-X)(WC-10Co)(X) composite coatings in NaCl medium. *Ceram. Int.* **2021**, *47*, 29410–29422. [[CrossRef](#)]
23. Liu, X.M.; Wang, H.B.; Feng, H.; Hu, H.X.; Chen, J.H.; Zhao, Z.; Wu, G.C.; Liu, C.; Lu, H.; Song, X.Y. On the enhanced wear resistance of ultra-coarse WC-Co cemented carbides by WCoB addition. *J. Alloy Compd.* **2022**, *894*, 162449. [[CrossRef](#)]
24. Qin, Y.Q.; Peng, Y.Q.; Tian, Y.; Luo, L.M.; Ma, Y.; Zan, X.; Zhu, X.Y.; Wu, Y.C. Effect of Y₂O₃ on microstructure and mechanical properties of WC-Co-cemented carbides prepared via solid-liquid doping method and spark plasma sintering. *Mater. Today Commun.* **2020**, *24*, 101096. [[CrossRef](#)]

25. Yang, T.E.; Xiong, J.; Sun, L.; Guo, Z.X.; Qin, K.C. Effects of nano- Al_2O_3 and nano- ZrO_2 on the microstructure, behavior and abrasive wear resistance of WC-8Co cemented carbide. *Rare Metals*. **2011**, *30*, 533–538. [[CrossRef](#)]
26. Kadyrzhanov, K.K.; Shlimas, D.I.; Kozlovskiy, A.L.; Zdorovets, M.V. Research of the shielding effect and radiation resistance of composite CuBi_2O_4 films as well as their practical applications. *J. Mater. Sci. Mater. Electron.* **2020**, *31*, 11729–11740. [[CrossRef](#)]
27. Zubar, T.I.; Usovich, T.I.; Tishkevich, D.I.; Kanafyev, O.D.; Fedkin, V.A.; Kotelnikova, A.N.; Panasyuk, M.I.; Kurochka, A.S.; Nuriev, A.V.; Idris, A.M.; et al. Features of galvanostatic electrodeposition of NiFe films with composition gradient: Influence of substrate characteristics. *Nanomaterials* **2022**, *12*, 2926. [[CrossRef](#)]
28. Li, J.F.; Cheng, J.G.; Wei, B.Z.; Chen, P.Q. Preparation and performance of ultrafine grained WC-10Co alloys with added La_2O_3 . *Ceram. Int.* **2019**, *45*, 3969–3976. [[CrossRef](#)]
29. Yang, Y.; Luo, L.M.; Zan, X.; Zhu, X.Y.; Zhu, L.; Wu, Y.C. Synthesis of Y_2O_3 -doped WC-Co powders by wet chemical method and its effect on the properties of WC-Co cemented carbide alloy. *Int. J. Refract. Met. Hard Mater.* **2020**, *92*, 105324. [[CrossRef](#)]
30. Cai, H.; Jing, W.W.; Guo, S.D.; Liu, L.; Ye, Y.; Wen, Y.; Wu, Y.X.; Wang, S.L.; Huang, X.; Zhang, J.B. Effects of micro/nano CeO_2 on the microstructure and properties of WC-10Co cemented carbides. *Int. J. Refract. Met. Hard Mater.* **2020**, *95*, 105432. [[CrossRef](#)]
31. Tokarewicz, M.; Gradzka-Dahlke, M. Review of Recent Research on AlCoCrFeNi High-Entropy Alloy. *Metals* **2021**, *11*, 1302. [[CrossRef](#)]
32. Liu, Y.; Li, X.F.; Zhou, J.H.; Fu, K.; Wei, W.; Du, M.; Zhao, X.F. Effects of Y_2O_3 addition on microstructures and mechanical properties of WC-Co functionally graded cemented carbides. *Int. J. Refract. Met. Hard Mater.* **2015**, *50*, 53–58. [[CrossRef](#)]
33. Zhao, Z.H.; Yao, G.; Luo, L.M.; Zan, X.; Xu, Q.; Wu, Y.C. Anisotropy and stability of the mechanical properties of the W alloy plate reinforced with Y-Zr-O particles and prepared by a wet chemical method. *Int. J. Refract. Met. Hard Mater.* **2021**, *99*, 105597. [[CrossRef](#)]
34. Trukhanov, S.V.; Trukhanov, A.V.; Vasiliev, A.N.; Balagurov, A.M.; Szymczak, H. Magnetic state of the structural separated anion-deficient $\text{La}_{0.70}\text{Sr}_{0.30}\text{MnO}_{2.85}$ manganite. *J. Exp. Theor. Phys.* **2011**, *113*, 819–825. [[CrossRef](#)]
35. Kozlovskiy, A.; Egizbek, K.; Zdorovets, M.V.; Ibragimova, M.; Shumskaya, A.; Rogachev, A.A.; Ignatovich, Z.V.; Kadyrzhanov, K. Evaluation of the efficiency of detection and capture of manganese in aqueous solutions of FeCeO_x nanocomposites doped with Nb_2O_5 . *Sensors* **2020**, *20*, 4851. [[CrossRef](#)] [[PubMed](#)]
36. Yang, Y.; Luo, L.M.; Zan, X.; Zhu, X.Y.; Zhu, L.; Wu, Y.C. Study on preparation and properties of WC-8Co cemented carbide doped with rare earth oxide. *Int. J. Refract. Met. Hard Mater.* **2021**, *98*, 105536. [[CrossRef](#)]
37. Chang, S.H.; Chen, S.L. Characterization and properties of sintered WC-Co and WC-Ni-Fe hard metal alloys. *J. Alloys Compd.* **2014**, *585*, 407–413. [[CrossRef](#)]
38. Lu, K.L.; Shen, C.J.; He, Y.Z.; Huang, S.; Ba, Y.E. Effect of solute elements (Cr, Mo, Fe, Co) on the adhesion properties of WC/Ni-based binder interface: A first-principles study. *Int. J. Refract. Met. Hard Mater.* **2021**, *98*, 105563. [[CrossRef](#)]
39. Fransson, E.; Gren, M.; Wahnstrom, G. Complexions and grain growth retardation: First-principles modeling of phase boundaries in WC-Co cemented carbides at elevated temperatures. *Acta Mater.* **2021**, *216*, 117128. [[CrossRef](#)]
40. Ghanbariha, M.; Farvizi, M.; Ebadzadeh, T.; Samiyan, A.A. Effect of ZrO_2 particles on the nanomechanical properties and wear behavior of AlCoCrFeNi- ZrO_2 high entropy alloy composites. *Wear* **2021**, *484*, 204032. [[CrossRef](#)]

Disclaimer/Publisher's Note: The statements, opinions and data contained in all publications are solely those of the individual author(s) and contributor(s) and not of MDPI and/or the editor(s). MDPI and/or the editor(s) disclaim responsibility for any injury to people or property resulting from any ideas, methods, instructions or products referred to in the content.